


Development of Dual Functional Nucleic Acid Delivery Nanosystem for DNA Induced Silencing of Bcl-2 Oncogene

This article was published in the following Dove Press journal:
International Journal of Nanomedicine

Somayah Karimi ^{1,*}
Mohamad Hassan Fouani^{2,*}
Ahmad Moshaii ¹
Maryam Nikkhah ²
Saman Hosseinkhani³
Reza Sheikhejad⁴

¹Department of Physics, Tarbiat Modares University, Tehran, Iran; ²Department of Nanobiotechnology, Tarbiat Modares University, Tehran, Iran; ³Department of Biochemistry, Tarbiat Modares University, Tehran, Iran; ⁴Department of Molecular Biology, Tofiq Daru Engineering-Research Co., Tehran, Iran

*These authors contributed equally to this work

Introduction: Cancer treatment using functionalized vehicles in order to block involved genes has attracted a remarkable interest. In this study, we investigated the cellular uptake and cytotoxic effects of three sizes of anti Bcl-2 DNAi-conjugated gold nanoparticles by MCF-7 cells.

Methods: Three different sizes of gold nanoparticles were synthesized by citrate reduction method and after characterization, the nanoparticles were functionalized by Bcl-2 targeted DNAi. Cell internalization of the nanoparticles was analyzed by atomic absorption spectroscopy and light microscopy. The cytotoxic effects of the nanoparticles were investigated by MTT assay, flow cytometry and RT-PCR of the target gene.

Results: While poor cell internalization of bare gold nanoparticles was observed, the results demonstrated that cellular uptake of DNAi-conjugated gold nanoparticles is completely size-dependent, and the largest nanoparticle (~42 nm) revealed the highest internalization rate compared to other sizes (~14 and ~26 nm). Experimental findings showed that the DNAi-conjugated gold nanoparticles induced apoptotic pathway by silencing of the targeted Bcl-2 gene. In addition, supplementary theoretical studies demonstrated that the 42 nm DNAi-conjugated gold nanoparticles have great photothermal conversion efficiency for treatment under external illumination and these nanoparticles can be induced further cytotoxic effect by approximately 10°C temperature elevations.

Conclusion: Remarkable photothermal properties of DNAi-conjugated 42 nm Au-NPs in parallel with their high cell internalization and cytotoxic effects introduce them as potential dual functional anticancer nanosystems.

Keywords: breast cancer, apoptosis, DNAi, Bcl-2, gold nanoparticles

Introduction

Cancer, one of the world's leading causes of death, is assisted by the improper expression of genes that regulate the cell cycle. Breast cancer is one of the most common cancers in women in which the treatment sufficiently depends on several parameters like the cancer type, extent of disease, and the age of patient.¹ The ability to change the normal pathway of apoptosis is a distinct property of cancer cells. A variety of chemotherapeutic drugs act on the elimination of target cells through activating common apoptotic pathways.² In most types of cancers, resistance to drug-induced apoptosis usually develops and leads to generation of chemotherapy-resistant cancer cells.³ Hence, efficient induction of apoptosis is a crucial approach for treatment of all the cancers.^{4,5}

Correspondence: Ahmad Moshaii;
Maryam Nikkhah
Tel +98 21 82 88 34 59;
+98 21 82 88 47 34
Email moshaii@modares.ac.ir;
m_nikkhah@modares.ac.ir

Bcl-2 protein family is a key regulator of cell death by suppressing or promoting apoptosis^{6–8} The Bcl-2 family is subdivided into two categories: antiapoptotic proteins (Bcl-2, Bcl-xL, Mcl-1, Bcl-w, and A-1), and proapoptotic proteins (Bax, Bak, Bik, Bad, Bid, HRK, BMF, NOXA, and PUMA).⁹ Bcl-2 oncogene is overexpressed in a wide range of human cancers including breast cancer cells.¹⁰ Based on the extensive evidences, it has been shown that by inhibition of Bcl-2 gene the cancer cells could be sensitized to standard therapies,¹¹ hence highlighting the significance of Bcl-2 oncogene as a potential therapeutic target in various human cancers.¹²

Nucleic acid-based drugs represent promising future therapeutics to target pathways and molecules involved in cancer and other genetic disorders.^{13,14} Plasmids¹⁵ and minivector DNAs¹⁶ can be implemented to repair defective genes, whilst small interfering RNA (siRNA)¹⁷ can be used to inhibit the expression of a specific messenger RNA (mRNA) exerting gene-silencing effects.^{12,18,19} A novel approach to inhibit transcription, termed DNA interference (DNAi), has been introduced by Rodriguez et al.^{12,20} DNAis are single stranded sequences, 20–34 bases long, tailored to bind to upstream DNA sequences of transcription initiation site. Hybridization of the DNAi oligonucleotide to its target region results in gene expression modulation at mRNA and protein levels.^{12,21}

Nucleic acid-based drugs require delivery vehicles capable of protecting its cargo from nucleases and delivering it to the target site.²² Cationic lipids and polymers as non-viral gene vectors have been used to form complexes with negatively charged DNA by means of electrostatic interactions.²³ Inorganic nanoparticles²⁴ as delivery vehicles offer several advantages to traditional vectors, such as tunable sizes and surface properties, multifunctional capabilities, and the ability to transfer the physical properties of the metal core to the medium.²⁵ Gold nanoparticles (Au-NPs), in particular, exhibit several features making them suitable carriers of “Nucleic acid-based” drugs.^{26–29} For instance, Au-NPs can be synthesized in a scalable fashion with low size dispersity.³⁰ Moreover, several functional groups such as nucleic acids and targeting agents could be placed on the particle’s surface resulting in functional diversity.^{31,32} Finally, the size and surface properties of Au-NPs can be easily modulated,³³ which in turn influence their cytotoxicity, biodistribution³⁴ and their in vivo excretion properties.³⁵ The interactions between conjugated Au-NPs and cell membranes have been suggested to govern bioavailability and efficiency of NPs internalization into the cancer cells.³⁶ It has been shown

that the uptake pattern depends on several parameters like the size, shape and surface chemistry of Au-NPs and the type of the cells.^{37–40} For instance, there are some positively charged regions on the cell surface, which could facilitate the uptake of negatively charged nanoparticles, and influence the entry rate into the cell.⁴¹ Theoretical calculations on spherical nanoparticles demonstrated that the maximal uptake rate by the cells occurred in the case of nanoparticle with the sizes of 50 nm.⁴² Also, some researchers investigated the interactions of different NPs with cell membranes and revealed that functionalized NPs with the sizes less than 100 nm enter the cells through clathrin-mediated endocytosis pathway.³⁷

Au-NPs due to their relatively low toxicity have attracted remarkable interest for photothermal therapy (PTT) of cancers.⁴³ These NPs can act as efficient converters of optical energy to thermal energy at the nanoscale times, especially when the optical excitation frequency is in resonance with their localized surface plasmon resonance (LSPR).⁴⁴ The temperature around and within a single Au-NP is related to its absorption cross-section and it can reach to a few tens of degrees.^{45,46} The rate of heat dissipations through particle–medium interfaces depends on the surrounding medium, particle size, surface chemistry and power of the illuminating laser sources.⁴⁷ When the NPs have functionalized with thermally sensitive molecules such as proteins and DNA, characterization of thermal dissipation is essential.⁴⁸

In this study, Au-NPs with the sizes of ~14, ~26, and ~42 nm conjugated with anti-Bcl-2 DNAi were efficiently delivered into MCF-7 cells (Figure 1). The largest size of the DNAi-conjugated Au-NPs (~42 nm) exhibited the most internalization rate, and the most toxicity against breast

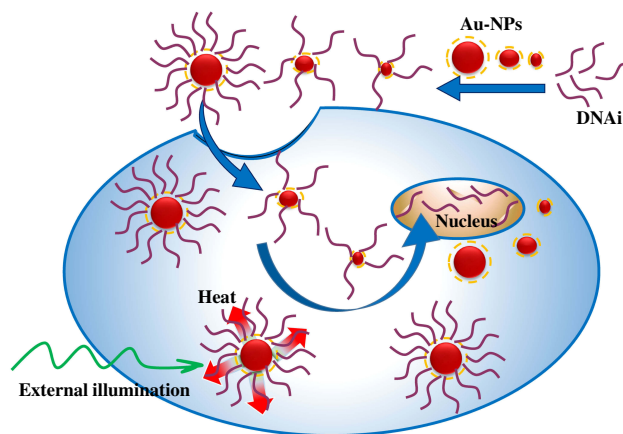


Figure 1 Schematic of DNAi-conjugated Au-NPs endocytosis into MCF-7 cells.

cancer cells. Further experiment performed to investigate the mechanism of cell death. The findings suggested that the anticancer effects of the DNAi conjugated Au-NPs were completely tuned by the size of nanoparticles. The results of the current work propose a new approach in efficient delivery of anti-Bcl-2 DNAi loaded Au-NPs to the breast cancer cells. Finally, we theoretically investigated the potential photothermal properties of DNAi-conjugated Au-NPs.

Materials and Methods

Reagents and Materials

Gold tetrachloroauric acid [HAuCl₄.3H₂O] and iodine [I₂] were purchased from Sigma Aldrich. Sodium phosphate monobasic [NaH₂PO₄], sodium phosphate dibasic [Na₂HPO₄], SDS [C₁₂H₂₅OSO₃Na], potassium iodide [KI], with molecular biology grade, were purchased from Acros. Tris (2-carboxyethyl) phosphine hydrochloride (TCEP) [C₉H₁₅O₆P.HCl] was supplied by Bio Basic (USA). Tri-sodium citrate dihydrate [Na₃C₆H₅O₇.2H₂O], sodium chloride [NaCl], and Potassium chloride [KCl] were obtained from Merck. Milli-Q water was used in preparation of all the solutions. All glasswares were cleaned with freshly prepared Aqua regia cleaning solution [HCl-HNO₃ (3:1)], rinsed with water and finally were oven-dried before using them.

The buffer solutions used for conjugation of DNAi and Au-NPs were prepared as follows: salting buffer (2 M of NaCl in 10 mM of phosphate buffer saline (PBS), pH 7.4), phosphate adjustment buffer (100 mM, pH 7).

The DNAi oligonucleotides as described by Tolcher et al⁴⁹ were provided by Reza Sheikhnejad. DNAi has the sequence of 5'-CACGCACGCGCATCCCCGCCCGTG-3'. The non-specific oligonucleotides purchased from Macrogen Company, South Korea, and the sequence is 5'-GCCATATAACAATAACAAGGC-3'. MCF-7 cells were purchased from Iranian Biological Resource Center. Medical ethics committee of Tarbiat Modares University approved cell experiments.

Statistical Analysis

Experimental data were plotted from three independent experiments and errors were presented as the mean standard deviation. Significance of differences between mean deviations was assessed using *t*-test; statistical significance of P values is shown as * for P values <0.05, ** for P values <0.01, *** for P values <0.001 and **** for P values <0.0001.

Synthesis of Citrate Stabilized Au-NPs in Different Sizes

Citrate-stabilized Au-NPs were synthesized using seeded-growth method.⁵⁰ At first, in order to synthesize gold seeds, sodium citrate aqueous solution (150 mL, 2.2 mM) was heated to boiling point. The reaction was conducted in a 250 mL three-necked round-bottomed flask which was connected to a condenser and placed in a hot oil bath. After continuous heating for 15 min under vigorous stirring, HAuCl₄ solution (1 mL, 25 mM) was quickly injected into the flask. The color of the solution changed from yellow to bluish gray and then to soft red. After 15 min, the solution was cooled slowly to 90°C and the resulting NPs were used as seeds. These nanoparticles (~14 nm) are coated with citrate ions and have negative surface potential. In order to synthesize Au-NPs of larger sizes, sodium citrate (1 mL, 60 mM) and HAuCl₄ solution (1 mL, 25 mM) were injected into the above-mentioned seed solution. After 30 min at 90°C, Au-NPs with ~26 nm diameter were obtained. Au-NPs with the size of ~42 nm were prepared by repeating the addition of sodium citrate (1 mL, 60 mM) and HAuCl₄ solution (1 mL, 25 mM) to seed solution for three times, and continuing the heating for 30 min at 90°C. The resulting Au-NP colloidal solutions were left undisturbed overnight and then stored at 4°C.

Functionalization of Gold Nanoparticles with DNAi

The synthesized Au-NPs were centrifuged for 10 min at 4°C (14 nm and 26 nm Au-NPs, 10,000g and 42 nm Au-NPs, 3500 g) and then were re-dispersed in Millipore water. The modification of Au-NPs with oligonucleotides was done based on Liu and Lu method.⁵¹ First, thiolated oligonucleotides (100 μM, 5 μL) were treated with freshly prepared TCEP solution (10 mM, 5 μL) and shaken gently for 1h at room temperature. Then, 500 μL of the prepared Au-NPs with various sizes was separately added to TCEP-treated thiolated DNAi and non-specific DNA. All tubes wrapped in foil and incubated on an orbital shaker at room temperature for at least 16h. Then, phosphate buffer (100 mM pH 7) was added to the Au-NPs solution to obtain a final phosphate buffer concentration of 9 mM. Subsequently, SDS was added to the reaction to reach the final SDS concentration of ~0.1% and shaking was continued for 30 more min. The salting buffer (2 M NaCl in 10 mM PBS pH 7) was divided into six doses, which

were added drop wisely to the reaction over the time course of 9h to reach the final concentration of 0.1 M NaCl in each sample. After the last step of salt addition, the solution was allowed to equilibrate for 1h and then the modified Au-NPs were collected by centrifugation and re-dispersed in the same volume of salting buffer (10 mM NaCl in 10 mM PBS pH7). At the end of the procedure, well-functionalized Au-NPs have the same red color as freshly synthesized unmodified Au-NPs. DNA-conjugated Au-NPs remain stable at 4°C for at least 2 months.

Physicochemical Properties of Au-NPs

UV–Vis absorption spectra of Au-NPs were recorded with a Perkin-Elmer 25 UV–Vis spectrometer in the wavelength range of 200 to 800 nm, with the resolution of 0.5 nm. Transmission Electron Microscopy (TEM) imaging was done with Zeiss-EM10C electron microscope at 100 kV. Samples were prepared by drop casting of the colloidal solution onto a Formvar-carbon coated Cu grid with 300 meshes and dried at room temperature. Dynamic Light Scattering (DLS) analysis was performed by a Zetasizer Nano Series device (Malvern), which is equipped with a 633 nm He-Ne laser at the angle of 173°. The hydrodynamic diameter, polydispersity index (PDI), and zeta potential values were measured by the DLS device. The electrophoretic mobility of DNAi-conjugated and bare Au-NPs on 1.5% Agarose gel were compared.

In order to assess the efficiency of modification of Au-NPs by DNAi, functionalized Au-NPs were precipitated by centrifugation and the absorbance of the supernatant was measured at 260 nm. Beer-Lambert's Law ($A=\epsilon cl$) was used to determine the concentration of free DNAi in supernatant, where ϵ is the molar absorptivity of DNA (0.027 mL (μg)⁻¹(cm)⁻¹).

Cytotoxicity Assay of DNAi Conjugated Au-NPs

Cytotoxic effects of the Au-NPs were assessed by MTT (3-(4,5-dimethylthiazol-2-yl)-2,5-diphenyltetrazolium bromide) (Sigma Aldrich) tetrazolium reduction assay. MCF-7 cells were seeded in 96-well plates at a density of 10⁵ cells/well, and allowed to grow under standard mammalian cell culture conditions. Then, the cells were treated with the 0.02 nM (particle concentration) of bare, DNAi conjugated Au-NPs of various sizes (14, 26 and 42 nm), non-specific DNA-conjugated Au-NPs and also 8 μM of doxorubicin, in serum-free culture medium for

1h. Subsequently, 10 μL of MTT solution (5 mg/mL in PBS) was added to each well and the plates were incubated for 3h at 37°C. Later on, the media were aspirated and 50 μL DMSO were added to dissolve the formazan crystals. Finally, an ELISA (μQuant , BIOTEK) plate reader instrument was used to quantify the absorbance of the samples at 570 nm.

Cell Uptake of Au-NPs

MCF-7 cells were grown at the density of 2×10^5 cells/well in 12-well plates under standard cell culture conditions. The following day, the culture media were replaced with fresh medium, and treated with 0.02 nM bare, DNAi-conjugated Au-NPs of various sizes (14, 26 and 42 nm), and non-specific DNA-conjugated Au-NPs with the size of 42 nm, for 1h. At the end of the treatment period, each well was washed three times with PBS. Subsequently, cells were incubated with 250 μL of the I₂: KI etching solution (0.34:2.04 mM) for 5 mins at room temperature. The etching solution was removed and each well was washed with 500 μL deionized distilled water.⁵² The cells were trypsinized (0.25% Trypsin-EDTA 1X, BIO-IDEA) at room temperature for 5 mins, and then equal volume of fetal bovine serum was added for trypsin inactivation. Detached cells were collected by centrifugation at 110 g for 5 mins. Then, the cells were lysed using a hypotonic solution (HEPES 10 mM, MgCl₂ 1.5 mM, KCl 10 mM, DTT 0.5 mM). The uptake of bare, DNAi-conjugated and non-specific DNA-conjugated Au-NPs by MCF-7 cells was quantified by Atomic Absorption Spectroscopy (AAS) (Shimadzu AA-670).

Inverted Phase-Contrast Microscopy

To investigate the localization of the bare and DNA-conjugated Au-NPs in MCF-7 cells, the treated cells were viewed using an inverted phase-contrast microscope (Axiophote, Zeiss, Germany) and photographed using a Nikon camera attached to the microscope. Right before imaging, the cells were incubated with 250 μL of the I₂: KI etching solution (0.34:2.04 mM) for 5 mins at room temperature. The etching solution was removed, and the cells were washed with 500 μL of deionized distilled water. The images were captured at 80 X magnification.

Annexin-V/PI Dual Staining Assay

Quantitative assessment of apoptosis was performed by flow-cytometry using fluorescein isothiocyanate (FITC) tagged Annexin V in conjunction with Propidium Iodide (BioLegend, San Diego, USA). Briefly, 70% confluent

MCF-7 cells in 12-well plates (2×10^5 cells/well), in triplicates, were separately treated with the 0.02 nM of bare, DNAi-conjugated, non-specific DNA-conjugated Au-NPs of various sizes and with $8 \mu\text{M}$ doxorubicin for 1h. After the treatment, the exposure media were collected and the cells were trypsinized and centrifuged at 4°C , 296 g for 5 mins. The cells were resuspended in the exposure media and collected by centrifugation at 4°C , 300g for 5 mins. The cells were washed twice with cold BioLegend cell staining buffer, and resuspended in Annexin V Binding Buffer to reach the cell density of 100 cells/mL. Subsequently, $5 \mu\text{L}$ of FITC Annexin V and $10 \mu\text{L}$ of PI solution was added to $100 \mu\text{L}$ of cell suspension followed by incubation at room temperature for 15 min in the dark. Finally, $400 \mu\text{L}$ Annexin V Binding Buffer was added to each test tube and analysis of the cells was performed immediately using an automated multicolor Flow Cytometer (BD Biosciences, USA). The number of events has been set to 10,000. Results were analyzed using Flowing 2.5.1 software.

RNA Isolation and Real-Time PCR

Analysis

MCF-7 cells were cultured at the density of 2×10^5 cells/well in 12-well plates in triplicates. The next day, cells were treated with DNAi-conjugated, non-specific DNA-conjugated and bare Au-NPs for 1h. Total RNA was extracted from treated cells using Trizol (Invitrogen) according to the manufacturer's instruction. Residual DNA was removed by DNase I (Fermentase) treatment. SYBR Premix Kit (Biofact, Korea, Cat#DQ385-10h) and Step One™ system (Applied Biosystems, USA) were used to perform quantitative RT-PCR of Bcl-2. Forward and reverse primers for Bcl-2 (NM_000657.2) were 5'-ACTTCGCCGAGATGTCCAGC-3' and 5'-TACAGTTCCACAAAGGCATCCCAG-3', respectively, and the forward and reverse primers for GAPDH (NM_002046.3) were 5'-GCCACATCGCTCAGACAC-3' and 5'-GGCAACAATATCCACTTTACCAG-3', respectively. Reactions were performed at 95°C for 15 min followed by 40 cycles of amplification (at 95°C for 10s, at 60°C for 25s and at 72°C for 30s). Melting curve stage was done at $95^\circ\text{C} \rightarrow 60^\circ\text{C}$ ($+0.3^\circ\text{C}$).

Calculation Method for Photothermal Efficiency

Based on the quantum size effect in NPs with sizes less than mean free path of electrons, a modified size-dependent dielectric function was considered.⁵³ Then, the absorption

cross-section of spherical NPs was calculated by Mie theory. Finally, temperature increase of NPs by external illumination was calculated based on the results of Baffou, et al.⁴⁶

Results and Discussion

Although it was shown theoretically that the optimal size of NPs for cell internalization is about 50 nm,⁴² there are discrepancies between experimental results about the size-dependency of NPs cell internalization.^{38,54-56} Here in, we examined cell internalization of DNAi-conjugated NPs with the sizes of ~14, ~26, and ~42 nm in diameter and the cytotoxic effects of these drug delivery nanosystems on MCF-7 cells were compared.

Functionalization and Characterization of NPs

The synthesized colloidal Au-NPs (14, 26, 42 nm) are stable because of the electrostatic repulsion between their surface negative charges due to capping of NPs by citrate ions. The loosely bound citrate layers could be easily exchanged with thiolated nucleic acid strands; their binding energy to the gold surface is ~45 kcal/mol.⁵⁰ Figure 2 demonstrates the relating plasmonic peaks of the bare and conjugated Au-NPs at three different sizes.

Compared to the bare counterparts, the grafting of oligonucleotides on the surface of NPs resulted in a red shift of around 2, 1, and 2 nm for nanoparticles with sizes 14, 26, 42 nm, respectively. The observed red shift in the absorption spectra can be attributed to the changes in the dielectric properties of the surrounding medium, by functionalization of Au-NPs with DNAi (Figure 2).⁵¹ Furthermore, the presence of oligonucleotides on the surface of Au-NPs increases the surface negative charge and lead to more stability of the colloidal nanoparticles (Figure 2D). The negatively charged phosphate backbone of DNA effectively protects nanoparticles against aggregation at high concentrations of salt.⁵⁷ While, addition of the same amount of salting buffer to bare NPs diminished the repulsive forces.⁵⁸

The size and morphology of DNAi-conjugated Au-NPs were examined by TEM and DLS method. TEM results clearly showed the monodisperse spherical Au-NPs with mean diameters of 13.64, 25.36, and 41.84 nm for samples denoted as 14 nm, 26 nm, and 42 nm, respectively. The results obtained using DLS (Table 1) are in consistent with TEM images confirming the narrow size distribution of the synthesized nanoparticles (Figure 3)

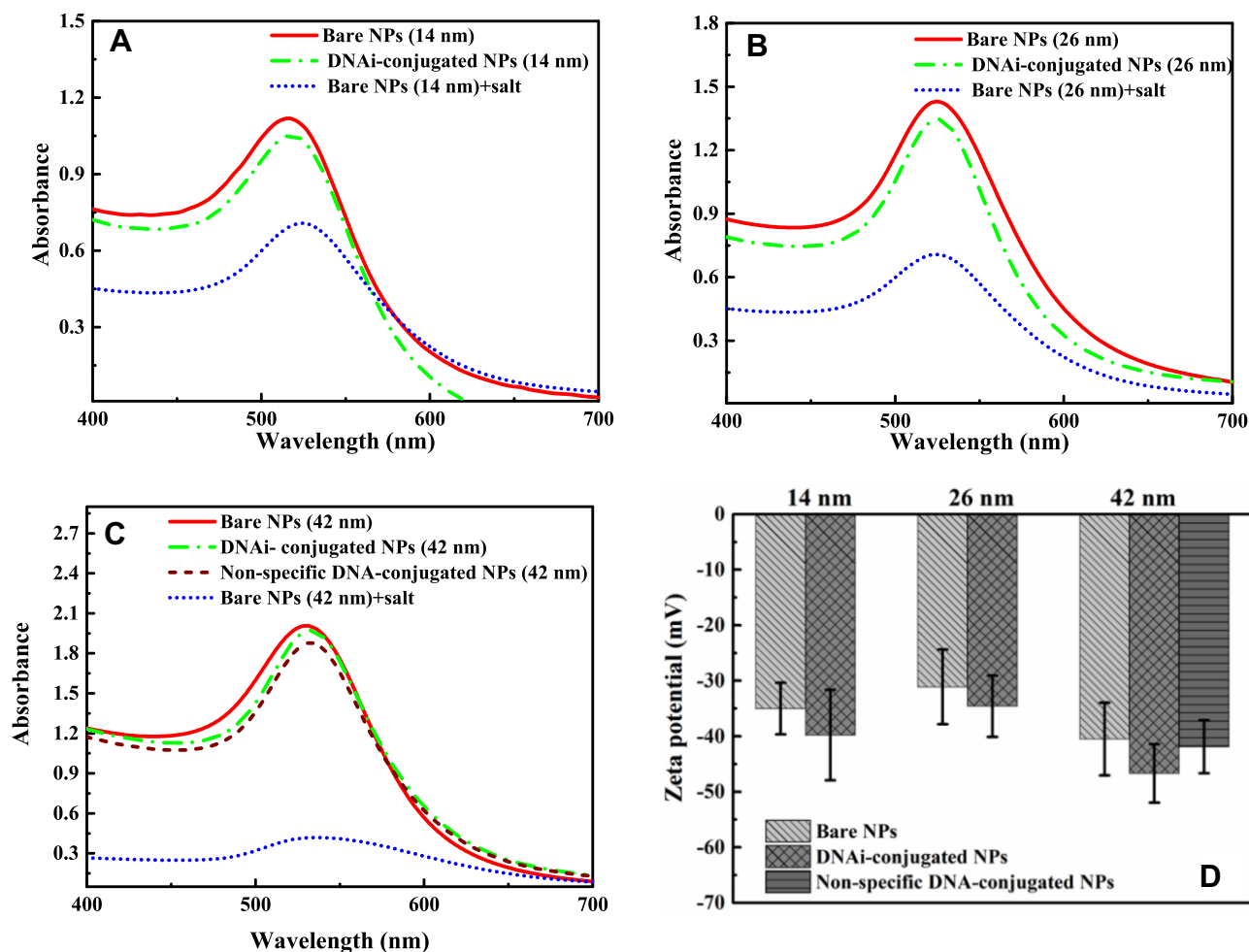


Figure 2 UV-Vis absorption spectra of colloidal Au-NPs before and after conjugation with DNAi for 14 nm Au-NPs (A), and 26 nm Au-NPs (B). UV-Vis absorption spectra of colloidal 42 nm Au-NPs before and after conjugation with DNAi and a non-specific DNA (C), and Zeta potentials of bare and conjugated Au-NPs at different sizes (D).

The electrophoretic mobility of the synthesized nanoparticles on agarose gel was studied. As seen in Figure 4A, compared to the bare Au-NPs DNAi-conjugated Au-NPs exhibited different electrophoretic pattern and moved faster on agarose gel confirming the conjugation of DNAi on the surfaces of the nanoparticles. Electrophoretic migration is dependent on the charge and size of the particles.⁵⁹ An increase in size and/or negative charge as a result of

DNAi-functionalization changes the migration profiles.⁶⁰ Figure 2D shows that DNAi-capped Au-NPs have an increased negative charge compared to bare Au-NP. As shown in Figure 4A, the smallest DNAi-conjugated Au-NPs, due to high ratio of surface charge to size, have the highest electrophoretic mobility. Conjugated Au-NPs with sizes of 26 nm and 42 nm have been retarded compared to 14 nm Au-NPs by their larger sizes. Retardation of 26 nm

Table 1 Average Diameter of the Au-NPs Determined by TEM and the Average Hydrodynamic Diameters and Polydispersity Indexes of Prepared Nanoparticles Have Been Measured by DLS Method

Au-NPs	Average Diameter of Functionalized NPs Measured by TEM (nm)	Average Diameter Measured by DLS (nm)		PDI	
		Bare NPs	Functionalized NPs	Bare NPs	Functionalized NPs
Au (14nm)	13.64±1.13	14.37±4.5	16.04±4.73	0.243	0.293
Au (26 nm)	25.36±2.94	26.91±6.83	27.09±6.69	0.125	0.116
Au (42 nm)	41.84±1.86	43.39±9.37	44.32±2.29	0.228	0.243

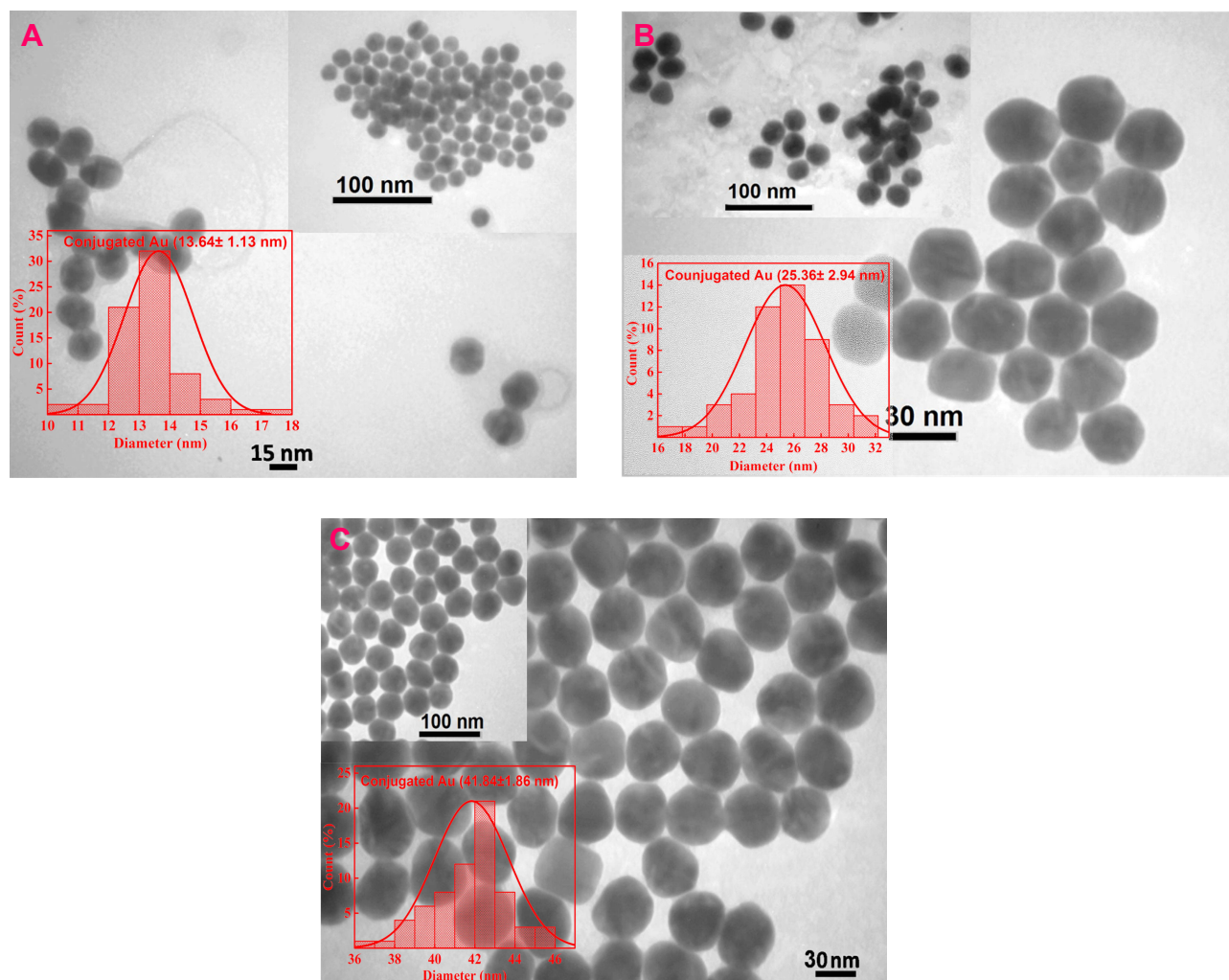


Figure 3 TEM images of DNAi-conjugated Au-NPs with the diameter of 14 nm (A), 26 nm (B), and 42 nm (C).

conjugated NPs compared to their 42 nm counterpart is related to their different surface charge density. The higher ratio of surface charge to size for 42 nm conjugated NPs has led to its more electrophoretic mobility.

In another experiment, the conjugation efficiencies of DNAi to Au-NPs at different sizes were compared. In this regard, after the final step of conjugation procedure, all samples were collected by centrifugation and the amount of unbound DNA in supernatant was determined by measuring the absorbance of the supernatants at 260 nm. The number of Au-NPs in each sample was estimated from the gold atom concentration determined by atomic absorption spectroscopy (AAS), average diameter of NPs based on TEM image and the geometrical calculations of the number of gold atoms in each NP. **Figure 4B** demonstrates the ratio of DNAi/particle for all three sizes of the NPs. As expected, the ratio of DNAi/Particle is the highest for

42 nm Au-NPs that provide the largest surface. Interestingly, the amount of DNAi per surface area (number of DNA strands/NP surface area) was calculated as 0.076, 0.346, and 0.758 (number/nm²) for 14, 26, and 42 nm Au-NPs, respectively. These findings show that the 42 nm NPs could be more efficiently conjugated to DNA.

Cytotoxic Effects of DNAi-Conjugated Au-NPs

Au-NPs can impose some levels of toxicity to biological systems. This toxicity is largely influenced by their characteristics such as their shape, size and surface chemistry.⁶¹ The DNAi loaded on the surface of Au-NPs is hypothesized to induce apoptosis through targeting Bcl-2 expression. In this study, MCF-7 cells were treated by DNAi-conjugated Au-NP and the viability of the cells was assessed by MTT assay (**Figure 5A**). Treating MCF-7 cells with free DNAi (500 and

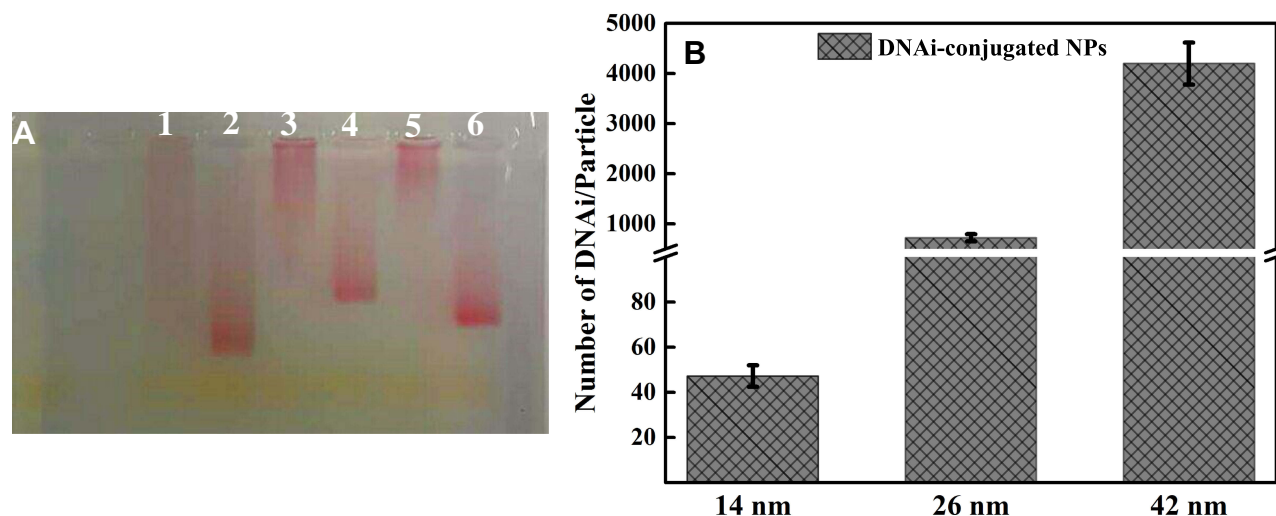


Figure 4 Agarose gel electrophoresis of bare 14 nm Au-NPs (lane 1), DNAi-conjugated 14 nm Au-NPs (lane 2), bare 26 nm (lane 3), DNAi-conjugated 26 nm Au-NPs (lane 4), bare 42 nm Au-NPs (lane 5), and DNAi-conjugated 42 nm Au-NPs (lane 6) (A), conjugation efficiencies of DNAi to Au-NPs as a function of Au-NPs size (B).

1000 nM) for 1h imposed no significant cytotoxic effects on the cells. Treating the cells with both the bare and DNAi-conjugated 14 nm Au-NPs showed mild toxicity on MCF-7 cells. Treatment of the cells with DNAi-conjugated Au-NPs sized 26 and 42 nm for 1h, results in cell viability of ~70% and ~38%, respectively. Treatment of the cells with non-specific DNA-conjugated 42 nm Au-NPs for 1h caused insignificant cytotoxicity. The potent cytotoxicity of 42 nm NPs was shown to be dose-dependent (Figure 5B and C). It is noteworthy that all the three different size of the bare Au-NPs exhibited almost the same level of cytotoxicity to the cells.

Cell Internalization of the NPs

It is believed that there are some positively charged patches in the cell membrane which facilitate the uptake of negatively charged nanoparticles.⁴¹ The adhesion of Au-NPs to the cell membranes strongly depends on the surface charge of nanoparticles and the type of the cells.⁵² MCF-7 cells were treated with the bare and DNAi-conjugated Au-NPs in different sizes and with non-specific DNA-conjugated 42 nm Au-NPs at a concentration of 0.02 nM for 1h. At the end of the treatment period, the cells were washed with the etching solution to eliminate the adsorbed NPs on the surface of the cells. Then, cell internalization of the Au-NPs was investigated and quantified by AAS. Our results demonstrate that cellular uptake of DNAi-conjugated Au-NPs was much higher in comparison with their bare Au-NPs counterparts (Figure 6a). DNAi presumably plays a critical role in cell internalization of the NPs. Furthermore, the largest DNAi-conjugated Au-NPs (42 nm) were internalized at higher amount (~30%) in comparison

with the other two DNAi-conjugated Au-NPs (14 nm and 26 nm), which were internalized at almost equal amount (~10%). The 42 nm non-specific DNA-conjugated Au-NPs were internalized to the cells with the efficiency of ~25%, that is approximately similar to the DNAi-conjugated NPs internalization rate.

Considering the highest concentration of the conjugated DNAi on the surface of the largest NPs (42 nm) (Figure 4B), and the highest rate of cell internalization of these NPs (Figure 6A), the superior cytotoxicity of these NPs can be explained. It should be emphasized that the observed effect is not merely dependent on the NPs' size, since all the bare NPs generally exhibited low internalization rate in comparison with their DNAi-conjugated Au-NPs counterparts (Figure 6A). Despite the remarkable internalization of non-specific DNA-conjugated Au-NPs in the cells, the cytotoxicity effects of these NPs were not significant.

To further investigate the internalization of the Au-NPs the treated cells were observed by an inverted phase-contrast microscopy. Au-NPs exhibit strong light scattering property which could be used as a powerful contrasting agent in their intracellular localization. For this purpose the cells were treated with 42 nm bare and DNA-conjugated Au-NPs and at the end of the treatment period, the cells were washed with the etching solution to eliminate the adsorbed NPs on the surface of the cells. Figure 6B clearly demonstrated that MCF-7 cells took up much more DNA-conjugated Au-NPs than bare NPs. Cell internalization followed by endosomal escape are definitely the most challenging barriers for drug

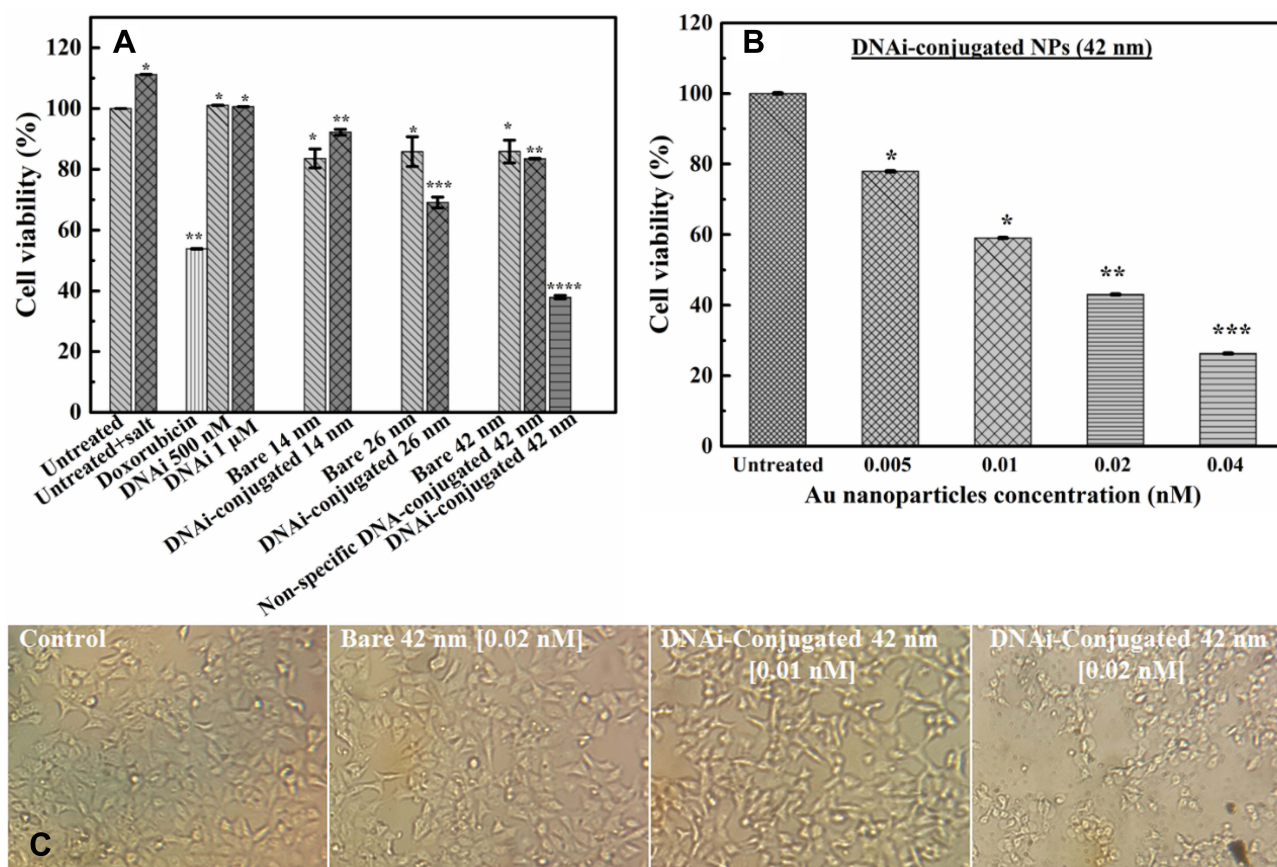


Figure 5 Cell viability of MCF-7 breast cancer cells treated by bare and DNAi-conjugated Au-NPs at different sizes, non-specific DNA-conjugated 42 nm Au-NPs, free DNAi, salting buffer and 8 μM of doxorubicin (A), cell viability of MCF-7 cells exposed to different concentrations of DNAi-conjugated 42 nm Au-NPs (B). Error bars are SD. Representative light microscopy imaging of MCF-7 cells treated by 42 nm bare and DNAi-conjugated Au-NPs (C). *P values <0.05, **P values <0.01, ***P values <0.001, ****P values <0.0001.

delivery. For instance, lipid nanoparticles loaded with siRNA exhibit low efficiency (1–2%) in escaping from endosomes and delivering their cargo into the cytosol.⁶² However, inorganic nanoparticles densely coated with highly oriented oligonucleotides designated as polyvalent nucleic acid-nanoparticles, represent one of the possible solutions for overcoming these problems.^{63,64} To date, investigations on cells (more than 50 cell lines, including primary cells) show that polyvalent nucleic acid-nanoparticles characterized with highly negative charge (zeta potential <-30 mV), do not need transfection agents or further surface functionalization to enter cells. Moreover, it has been assessed DNA surface density is directly proportional to the rate of cellular uptake of these particles; higher DNA densities lead to elevated rates of cellular uptake.⁶⁵ In addition, extensive evidence exists in support of the fact that high densities of DNA results in the recruitment of scavenger receptors, facilitating endocytosis of the nanoparticle.^{65,66} Furthermore, the enzymatic degradation of the nucleic acid conjugates is inhibited as a result of the ion cloud accompanying the shell of densely packed

oligonucleotide as well as the steric inhibition at the surface of the nanoparticle.^{67,68}

Apoptosis Induction by DNAi-Conjugated Au-NPs

As the Bcl-2 DNAi is supposed to induce apoptosis, the mechanism of the cell death induced by DNAi-conjugated and non-specific DNA-conjugated Au-NPs was investigated by Annexin V/PI staining of the cells followed by flowcytometry. As shown in Figure 7A, treatment of the cells with 42 nm DNAi-conjugated Au-NPs has led to 76.21% apoptotic cells, which is significantly higher than the bare 42 nm Au-NPs treated group. Therefore, blocking Bcl-2 anti-apoptotic proteins can promote apoptosis and suppress the growth of the cancer cells. Also, treatment of the cells with the non-specific DNA-conjugated demonstrated 70% live cells, which is comparable with the effect of the bare NPs. The percentages of apoptotic cells are depicted in Figure 7B.

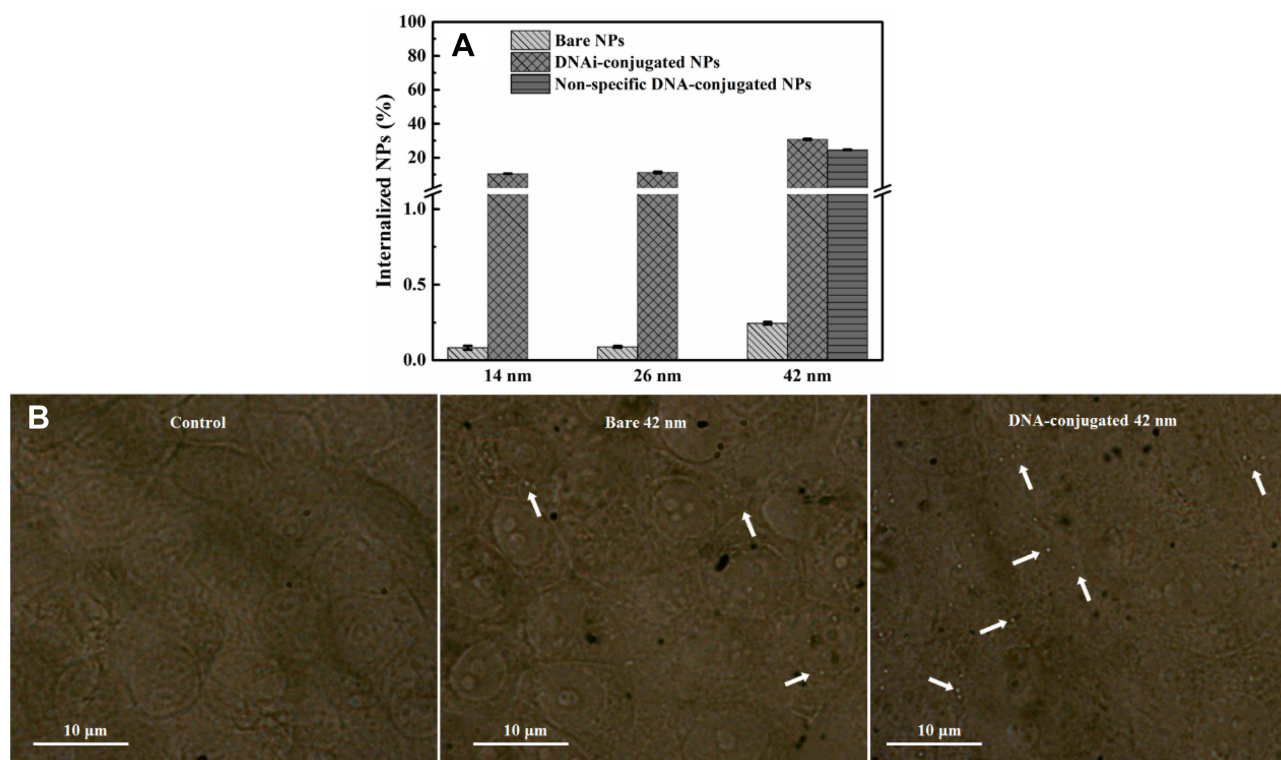


Figure 6 Cellular uptake of bare, DNAi-conjugated, and non-specific DNA-conjugated Au-NPs by MCF-7 breast cancer cells within 1h of quantification using atomic absorption spectroscopy (A). The inverted phase-contrast microscopy images of MCF-7 cells treated by 42 nm bare, the corresponding DNA-conjugated Au-NPs and untreated cells. Arrows indicate the Au-NPs (B).

Gene silencing function of DNAi-conjugated 42 nm Au-NPs was further assessed at the mRNA level using RT-PCR. Results shown in Figure 7C indicated that the 42 nm DNAi-conjugated 42 nm Au-NPs significantly diminished the expression of Bcl-2 gene compared to bare NPs. Exposure to 0.01 and 0.02 nM of DNAi-conjugated NPs causes a concentration-dependent decrease in the relative expression of Bcl-2 gene. To the best of our knowledge, few reports exist on DNAi delivery to the cell with the aim of suppressing the transcription of target genes.^{12,20,49,69} For instance, Rodriguez et al¹² reported efficient antiproliferative activity of the PNT100 DNAi through silencing of Bcl-2 gene. Liposomes were utilized to deliver PNT100 to breast and melanoma cell lines where 67–76% and 42–65% of growth inhibition were achieved, respectively, at 10 μ M of PNT 100 after 72h. In a separate study, Al-Katib et al presented an enhanced liposomal formulation of PNT 100, designated PNT2258. Exposure of follicular small cleaved cell lymphoma (WSU-FSCCL) cells to 2.5 μ M of PNT2258 successfully downregulated the Bcl-2 mRNA level and protein expression, resulting in the activation of apoptotic pathways in WSU-FSCCL cells 48h following transfection.²⁰ In the present study, prominent Bcl-2 gene silencing in MCF-7 cells

was observed by treatment at 0.02 nM of DNAi-conjugated Au-NPs for 1h. By considering the number of DNAi bound to the surface of each NP (Figure 4B), the working concentration of DNAi for 14, 26, and 42 nm conjugated NPs are 0.94, 14.5, and 84 nM, respectively. The presented data here introduced the synthesized DNAi-conjugated Au-NPs as a powerful candidate for silencing of Bcl-2 gene.

Size-Tunable Photothermal Conversion Efficiencies of Gold Nanoparticles

Metal NPs irradiated at resonant frequencies dissipate energy into heat with a high efficiency. The distinct properties of Au-NPs like low toxicity in cells have also led to the development of photothermal therapy for cancer treatment. Since the selected DNAi-conjugated Au-NPs efficiently indicated drug delivery results, we investigated theoretically potential of these NPs for photothermal therapy in cancer treatment. Conjugated spherical Au-NPs under external illumination can contribute to confine the temperature increment at the close vicinity of the NPs. Therefore, these NPs can provide local heating of cancer cells without heating of the surrounding healthy cells.⁷⁰ Based on the enhanced absorbance cross-sections of metal

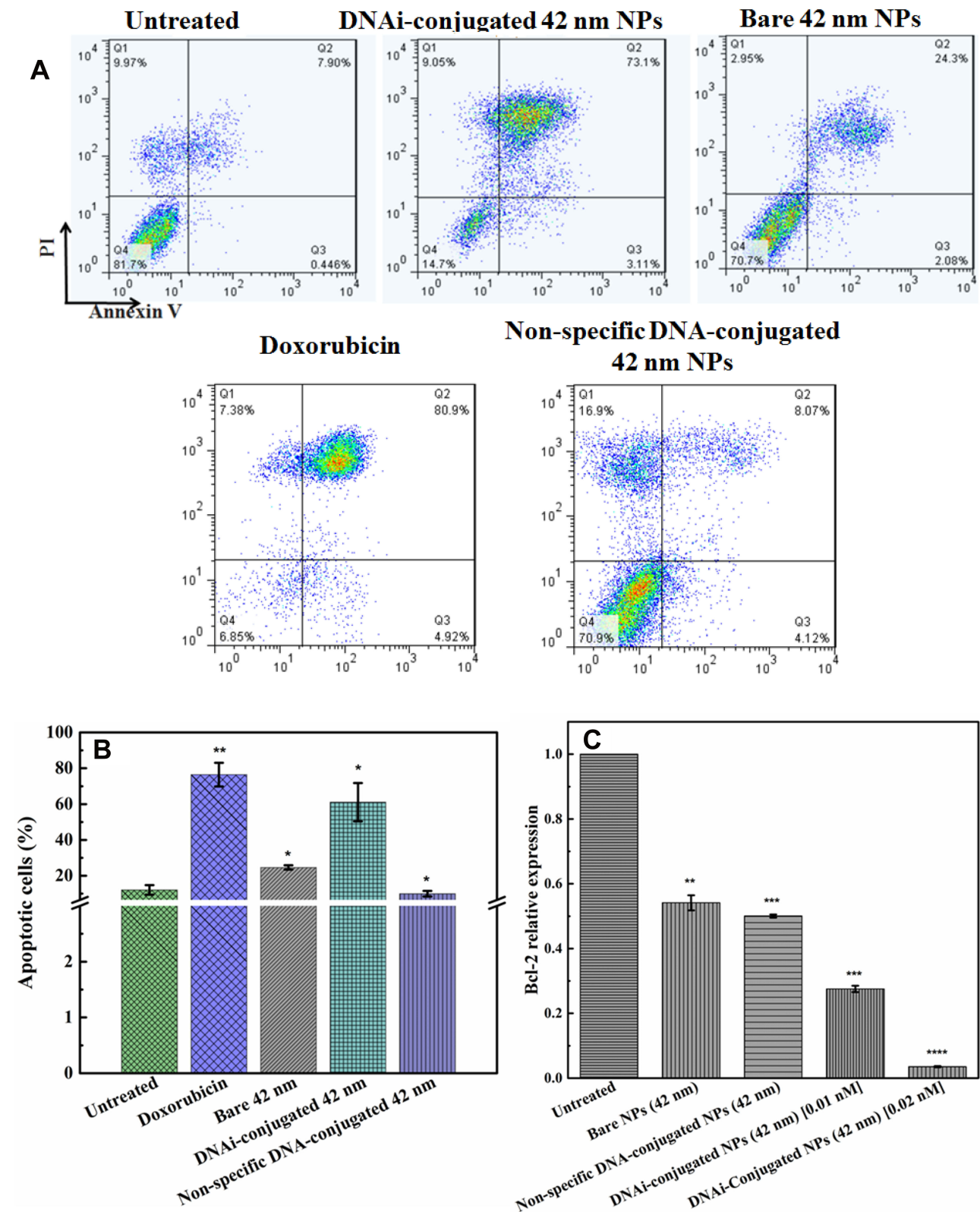


Figure 7 AnnexinV/PI Flow cytometry of untreated MCF-7 cells, DNAi-conjugated 42nm Au-NPs, bare 42nm Au-NPs, non-specific DNA-conjugated 42nm Au-NPs, and doxorubicin treated cells (A), corresponding apoptotic cells percentages (B), Bcl-2 relative expression in the cells treated with bare and non-specific DNA-conjugated 42 nm Au-NPs with 0.02 nM concentration and the DNAi-conjugated Au-NPs at two different concentrations (C). Error bars are SD. *P values<0.05, **P values <0.01, ***P values <0.001, ****P values <0.0001.

nanoparticles,⁷¹ the temperature around and within a single Au-NP could be up to a few tens degrees.⁴⁵ In this study, based on the result of ref.,⁴⁶ a single spherical Au-NPs with radius of R immersed in water and due to the hydrophilic nature and negative charge of DNA, a perfect interface conductivity was assumed. The degradation temperature of DNA changes in dry or aqueous surrounding medium.⁵⁹ In aqueous solution, the DNA degradation temperature is 100–110°C.⁵⁹ Therefore, we considered DNAi-conjugated Au-NPs, with no degradation, to be uniformly illuminated by continuous wave (cw) green laser (532 nm wavelength) with the irradiance (I) of 1 mW/μm^{2,45} From the energy conservation equation and considering boundary conditions at the gold water interface in the steady state regime, we can obtain the temperature increment inside and outside of the NP as follows:⁴⁶

$$T(r) = \frac{P_0}{4\pi\kappa_w r} \quad \text{for } r > R$$

$$T(r) = \frac{P_0}{4\pi\kappa_w R} \left\{ 1 + \frac{1}{2\gamma} \left(1 - \frac{r^2}{R^2} \right) + \lambda_k \right\} \quad \text{for } r < R \quad (1)$$

where P_0 is the heat power dissipated in the NP, $\gamma = \kappa_{gold}/\kappa_w \approx 558$ is a dimensionless constant in which $\kappa_w = 0.563\text{W}/\text{m}^\circ\text{K}$ is the thermal conductivity of water, and $\kappa_{gold} = 314\text{W}/\text{m}^\circ\text{K}$ is the thermal conductivity of gold. Also, $\lambda_k = \kappa_w/gR$ is a dimensionless constant in which g is the interface conductivity. Due to infinite conductivity of DNA on the surface, λ_k was set to zero. As $\gamma \gg 1$, one can usually consider the inside temperature of NP is uniform and equals to the following equation:⁴⁶

$$T(r) = \frac{P_0}{4\pi\kappa_w R} = \frac{\sigma_{abs} I}{4\pi\kappa_w R} \quad (2)$$

where σ_{abs} is the optical absorption cross-section of NP that can be obtained from Mie theory as follows:⁵³

$$\sigma_{abs} = \sigma_{ext} - \sigma_{scat}$$

$$= \frac{2\pi}{k^2} \left(\sum_{n=1}^{\infty} (2n+1) \text{Re}\{a_n + b_n\} - \sum_{n=1}^{\infty} (2n+1) \left\{ |a_n|^2 + |b_n|^2 \right\} \right) \quad (3)$$

where σ_{ext} and σ_{scat} are the extinction and scattering cross-section, respectively. The scattering coefficients a_n and b_n are:

$$a_n = \frac{\mu m^2 j_n(mx) [x j_n(x)]' - \mu_1 j_n(x) [mx j_n(mx)]'}{\mu m^2 j_n(mx) [x h_n^{(1)}(x)]' - \mu_1 h_n^{(1)}(x) [mx j_n(mx)]'} \quad (4)$$

$$b_n = \frac{\mu_1 j_n(mx) [x j_n(x)]' - \mu j_n(x) [mx j_n(mx)]'}{\mu_1 j_n(mx) [x h_n^{(1)}(x)]' - \mu h_n^{(1)}(x) [mx j_n(mx)]'} \quad (5)$$

where the prime indicates differentiation with respect to the argument in the parentheses. The size parameter x and the relative refractive index m are obtained as:

$$x = kR = \frac{2\pi n_{medium}}{\lambda} R, m = \frac{n_{sphere}}{n_{medium}}$$

with n_{sphere} and n_{medium} as the refractive indices of the Au-NP and its surrounding medium, respectively. Also, λ is the wavelength of the incident light, μ_L and μ are the permeability coefficients of the NP and the surrounding medium, which both are assumed to be unity (a reasonable assumption for the high frequencies in the visible region). $n_{sphere} = \sqrt{\epsilon(\omega, R)\mu_1}$ is the size-dependent refractive index of nanoparticles with sizes less than mean free path of electron (for gold 42 nm), that $\epsilon(\omega, R)$ is modification of the Drude dielectric model for Au-NP with the quantum size effects.⁵³ Therefore, the size-dependent dielectric function for nanoparticles can be obtained from:

$$\epsilon(\omega, R) = \epsilon_{JC}(\omega) + \frac{\omega_p^2}{\omega^2 + \gamma_{free}\omega} - \frac{\tilde{\omega}_p^2(R)}{\omega^2 + \gamma(R)\omega} \quad (6)$$

where ϵ_{JC} is the dielectric function obtained from the Johnson-Christy experiment,⁷² and $\omega_p = 9.08\text{eV}$ is the bulk plasma frequency and $\gamma_{free} = 0.0708\text{eV}$ is the damping constant of the electrons,⁷² $\omega_p(R)$ and $\gamma(R)$ are the size-dependent plasma frequency and damping term, respectively. It should be mentioned that $\epsilon(\omega) = \epsilon_{JC}(\omega)$ was used for nanoparticles with sizes larger than mean free path of electron ($2R > 42$ nm). In the following, the Mie theory (Eq. 3) will be used whenever a calculation of the absorption cross-section is required. Figure 8A demonstrates the absorption and scattering cross-sections of different sizes of Au-NPs calculated at resonance wavelength with incident light (532 nm).

Au-NPs with diameter larger than 100 nm, due to the increment of scattering cross-section, have no efficiency for photothermal purposes. As shown in Figure 8A, the NPs with diameter approximately 100 nm have comparable absorption and scattering cross-section. Therefore, we introduced an efficiency factor as $\eta = \sigma_{abs}/\sigma_{scat}$ for heating of Au-NPs under external illumination. This parameter was calculated for different sizes in Figure 8B. Owing to the high heating efficiency of NPs with sizes smaller than 50 nm, these NPs can efficiently absorb remarkable portion of external illumination. During the light absorption process, distribution of oscillating electrons changes very fast at a time scale of $\tau_e \sim 100$ fs.⁴⁶ In this time scale, the electrons of NP experience

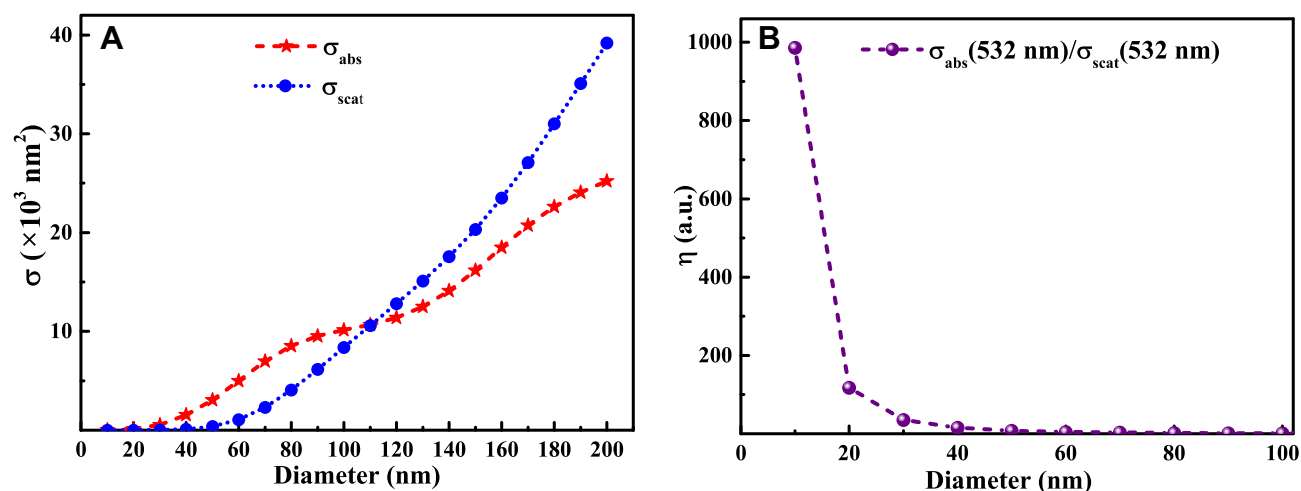


Figure 8 Absorption and scattering cross-sections at 532 nm for different sizes of Au-NPs immersed in water (A), photothermal efficiency of different sizes of Au-NPs (B).

a nonequilibrium state, while the temperature of the lattice (phonons) remains unchanged. The oscillating electrons of the nanoparticles transfer the kinetic energy into heat through the particle lattice or other electrons.⁴⁵ The electron–phonon scattering time is at the scale of 1.7 ps, and this interaction is size-independent. While phonon–phonon interactions with the surrounding medium happen at a time scale of 100–380 ps.⁴⁵ As the NP return to its initial temperature, heat dissipation through particle–medium interfaces is dependent on the medium, particle size, and laser source.⁴⁷ The steady-state temperature of different Au-NPs under cw illumination by using Eq. 1 was calculated and presented in Figure 9.

For nanoparticles with sizes smaller than 40 nm (sizes comparable with mean free path of electrons in gold), the size effect or collisions of electrons act as an important factor

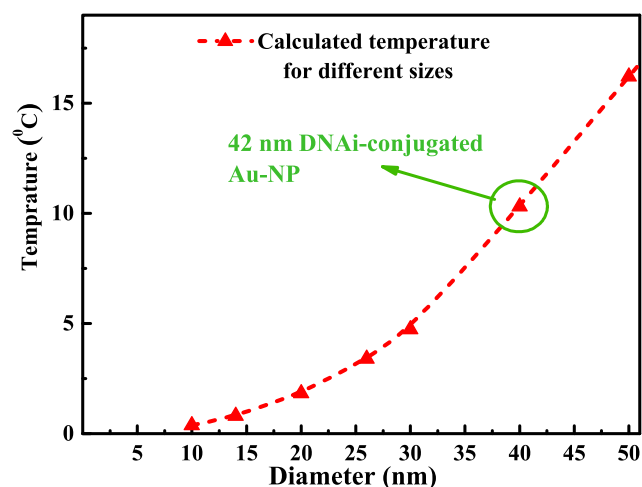


Figure 9 Temperature on the surface of a DNAi-conjugated Au-NP under cw illumination.

influencing the heat transfer. Also, the optimal diameter of NPs for efficient heating induced by a femtosecond-pulsed illumination was suggested to be 40 nm.⁴⁶ Figure 9 demonstrates the promising potential of Au-NPs with sizes smaller than 50 nm for photothermal treatment of cancer cells. Among the selected NPs in this study, the highest temperature increment was shown on the surface of DNAi-conjugated 42 nm Au-NPs. This property in parallel with the high cell internalization and cytotoxic effects of DNAi-conjugated 42 nm Au-NPs introduce them as potential dual functional anticancer nanosystems.

Conclusions

In conclusion, the efficiency of a specific DNAi on silencing of Bcl-2 gene expression by using different sizes of spherical Au-NPs as the carriers was investigated. The experimental findings demonstrate that the designed nanosystem can efficiently induce apoptosis in MCF-7 cells. In addition to the superior cytotoxic properties of the functionalized 42nm Au-NPs against breast cancer cells, considerable photothermal properties are expected for this size of Au-NPs, supported by the theoretical plasmonic calculations. Consequently, our finding suggests that the DNAi-conjugated 42 nm Au-NPs might be a promising therapeutic element for breast cancer treatment.

Acknowledgment

The authors acknowledge the financial support of this work by research council of Tarbiat Modares University (TMU).

Author Contributions

All authors contributed to data analysis, drafting and revising the article, gave final approval of the version to be

published, and agree to be accountable for all aspects of the work.

Disclosure

The authors declare that they have no known competing financial and non-financial interests that could have appeared to influence the work reported in this paper.

References

- Allemani C, Matsuda T, Di Carlo V, et al. Global surveillance of trends in cancer survival 2000–14 (CONCORD-3): analysis of individual records for 37 513 025 patients diagnosed with one of 18 cancers from 322 population-based registries in 71 countries. *Lancet*. 2018;391(10125):1023–1075. doi:10.1016/S0140-6736(17)33326-3
- Hannun YA. Apoptosis and the dilemma of cancer chemotherapy. *Blood*. 1997;89(6):1845–1853. doi:10.1182/blood.V89.6.1845
- Cross D, Burmester JK. Gene therapy for cancer treatment: past, present and future. *Clin Med Res*. 2006;4(3):218–227. doi:10.3121/cmr.4.3.218
- Thundimadathil J. Cancer treatment using peptides: current therapies and future prospects. *J Amino Acids*. 2012;2012:967347.
- Gui C, Cui D-X. Functionalized gold nanorods for tumor imaging and targeted therapy. *Cancer Biol Med*. 2012;9(4):221.
- Czabotar PE, Lessene G, Strasser A, Adams JM. Control of apoptosis by the BCL-2 protein family: implications for physiology and therapy. *Nat Rev Mol Cell Biol*. 2014;15(1):49. doi:10.1038/nrm3722
- Wilson T, Longley D, Johnston P. Chemoresistance in solid tumours. *Ann Oncol*. 2006;17(suppl_10):x315–x324. doi:10.1093/annonc/mdl280
- Lang J-Y, Hsu JL, Meric-bernstam F, et al. BikDD eliminates breast cancer initiating cells and synergizes with lapatinib for breast cancer treatment. *Cancer Cell*. 2011;20(3):341–356. doi:10.1016/j.ccr.2011.07.017
- Youle RJ, Strasser A. The BCL-2 protein family: opposing activities that mediate cell death. *Nat Rev Mol Cell Biol*. 2008;9(1):47. doi:10.1038/nrm2308
- Tawfik K, Kimler BF, Davis MK, Fan F, Tawfik O. Prognostic significance of Bcl-2 in invasive mammary carcinomas: a comparative clinicopathologic study between “triple-negative” and non-“triple-negative” tumors. *Hum Pathol*. 2012;43(1):23–30. doi:10.1016/j.humpath.2011.04.011
- Tabuchi Y, Matsuoka J, Gunduz M, et al. Resistance to paclitaxel therapy is related with Bcl-2 expression through an estrogen receptor mediated pathway in breast cancer. *Int J Oncol*. 2009;34(2):313–319.
- Rodrigueza WV, Woolliscroft MJ, Ebrahim A-S, et al. Development and antitumor activity of a BCL-2 targeted single-stranded DNA oligonucleotide. *Cancer Chemother Pharmacol*. 2014;74(1):151–166. doi:10.1007/s00280-014-2476-y
- Mulligan RC. The basic science of gene therapy. *Science*. 1993;260(5110):926–932. doi:10.1126/science.8493530
- Li J, Liang H, Liu J, Wang Z. Poly (amidoamine)(PAMAM) dendrimer mediated delivery of drug and pDNA/siRNA for cancer therapy. *Int J Pharm*. 2018;546(1–2):215–225. doi:10.1016/j.ijpharm.2018.05.045
- Bonadio J, Smiley E, Patil P, Goldstein S. Localized, direct plasmid gene delivery in vivo: prolonged therapy results in reproducible tissue regeneration. *Nat Med*. 1999;5(7):753. doi:10.1038/10473
- Zhao N, Fogg J, Zechiedrich L, Zu Y. Transfection of shRNA-encoding Minivector DNA of a few hundred base pairs to regulate gene expression in lymphoma cells. *Gene Ther*. 2011;18(3):220. doi:10.1038/gt.2010.123
- Behlke MA. Progress towards in vivo use of siRNAs. *Mol Ther*. 2006;13(4):644–670. doi:10.1016/j.ymthe.2006.01.001
- Young RL, Korsmeyer SJ. A negative regulatory element in the bcl-2 5'-untranslated region inhibits expression from an upstream promoter. *Mol Cell Biol*. 1993;13(6):3686–3697. doi:10.1128/MCB.13.6.3686
- Duan H, Xiang H, Ma L, Boxer LM. Functional long-range interactions of the IgH 3' enhancers with the bcl-2 promoter region in t (14; 18) lymphoma cells. *Oncogene*. 2008;27(53):6720. doi:10.1038/onc.2008.286
- Ebrahim AS, Kandouz M, Liddane A, et al. PNT2258, a novel deoxyribonucleic acid inhibitor, induces cell cycle arrest and apoptosis via a distinct mechanism of action: a new class of drug for non-Hodgkin's lymphoma. *Oncotarget*. 2016;7(27):42374. doi:10.18632/oncotarget.9872
- Hoffman AR, Hu JF. Directing DNA methylation to inhibit gene expression. *Cell Mol Neurobiol*. 2006;26(4–6):423–436. doi:10.1007/s10571-006-9057-5
- Sokolova V, Epple M. Inorganic nanoparticles as carriers of nucleic acids into cells. *Angew Chem Int Ed*. 2008;47(8):1382–1395. doi:10.1002/(ISSN)1521-3773
- Zhao Z, Li Y, Shukla R, et al. Development of a biocompatible copolymer nanocomplex to deliver VEGF siRNA for triple negative breast cancer. *Theranostics*. 2019;9(15):4508. doi:10.7150/thno.34314
- Arsianti M, Lim M, Marquis CP, Amal R. Assembly of polyethylenimine-based magnetic iron oxide vectors: insights into gene delivery. *Langmuir*. 2010;26(10):7314–7326. doi:10.1021/la9041919
- Ding Y, Jiang Z, Saha K, et al. Gold nanoparticles for nucleic acid delivery. *Mol Ther*. 2014;22(6):1075–1083. doi:10.1038/mt.2014.30
- Park K, Lee S, Kang E, Kim K, Choi K, Kwon IC. New generation of multifunctional nanoparticles for cancer imaging and therapy. *Adv Funct Mater*. 2009;19(10):1553–1566. doi:10.1002/adfm.v19:10
- Khamehchian S, Nikkha M, Madani R, Hosseinkhani S. Enhanced and selective permeability of gold nanoparticles functionalized with cell penetrating peptide derived from maurocalcine animal toxin. *J Biomed Mater Res A*. 2016;104(11):2693–2700. doi:10.1002/jbma.35806
- Abdel-rashid RS, Omar SM, Teiama MS, Khairy A, Magdy M, Anis B. Fabrication of gold nanoparticles in absence of surfactant as in vitro carrier of plasmid DNA. *Int J Nanomedicine*. 2019;14:8399. doi:10.2147/IJN.S226498
- Vio V, Riveros AL, Tapia-bustos A, et al. Gold nanorods/siRNA complex administration for knockdown of PARP-1: a potential treatment for perinatal asphyxia. *Int J Nanomedicine*. 2018;13:6839. doi:10.2147/IJN.S175076
- Daniel M-C, Astruc D. Gold nanoparticles: assembly, supramolecular chemistry, quantum-size-related properties, and applications toward biology, catalysis, and nanotechnology. *Chem Rev*. 2004;104(1):293–346.
- Bowman M-C, Ballard TE, Ackerson CJ, Feldheim DL, Margolis DM, Melander C. Inhibition of HIV fusion with multivalent gold nanoparticles. *J Am Chem Soc*. 2008;130(22):6896–6897. doi:10.1021/ja710321g
- Ryan JA, Overton KW, Speight ME, et al. Cellular uptake of gold nanoparticles passivated with BSA–SV40 large T antigen conjugates. *Anal Chem*. 2007;79(23):9150–9159. doi:10.1021/ac0715524
- Kim ST, Saha K, Kim C, Rotello VM. The role of surface functionality in determining nanoparticle cytotoxicity. *Acc Chem Res*. 2013;46(3):681–691. doi:10.1021/ar3000647
- De Jong WH, Hagens WI, Krystek P, Burger MC, Sips AJ, Geertsma RE. Particle size-dependent organ distribution of gold nanoparticles after intravenous administration. *Biomaterials*. 2008;29(12):1912–1919. doi:10.1016/j.biomaterials.2007.12.037
- Wang B, He X, Zhang Z, Zhao Y, Feng W. Metabolism of nanomaterials in vivo: blood circulation and organ clearance. *Acc Chem Res*. 2012;46(3):761–769. doi:10.1021/ar2003336

36. Zhao J, Stenzel MH. Entry of nanoparticles into cells: the importance of nanoparticle properties. *Polym Chem.* 2018;9(3):259–272. doi:10.1039/C7PY01603D
37. Chithrani BD, Chan WC. Elucidating the mechanism of cellular uptake and removal of protein-coated gold nanoparticles of different sizes and shapes. *Nano Lett.* 2007;7(6):1542–1550. doi:10.1021/nl070363y
38. Jiang W, Kim BY, Rutka JT, Chan WC. Nanoparticle-mediated cellular response is size-dependent. *Nat Nanotechnol.* 2008;3(3):145. doi:10.1038/nnano.2008.30
39. Lu F, Wu SH, Hung Y, Mou CY. Size effect on cell uptake in well-suspended, uniform mesoporous silica nanoparticles. *Small.* 2009;5(12):1408–1413. doi:10.1002/sml.200900005
40. Zhang S, Li J, Lykotra G, Bao G, Suresh S. Size-dependent endocytosis of nanoparticles. *Adv Mater.* 2009;21:419–424. doi:10.1002/adma.v21:4
41. Chithrani BD, Ghazani AA, Chan WC. Determining the size and shape dependence of gold nanoparticle uptake into mammalian cells. *Nano Lett.* 2006;6(4):662–668. doi:10.1021/nl052396o
42. Yuan H, Zhang S. Effects of particle size and ligand density on the kinetics of receptor-mediated endocytosis of nanoparticles. *Appl Phys Lett.* 2010;96(3):033704. doi:10.1063/1.3293303
43. Tan G, Onur MA. Cellular localization and biological effects of 20nm-gold nanoparticles. *J Biomed Mater Res A.* 2018;106(6):1708–1721. doi:10.1002/jbm.a.v106.6
44. Govorov AO, Richardson HH. Generating heat with metal nanoparticles. *Nano Today.* 2007;2(1):30–38. doi:10.1016/S1748-0132(07)70017-8
45. Jiang K, Smith DA, Pinchuk A. Size-dependent photothermal conversion efficiencies of plasmonically heated gold nanoparticles. *J Phys Chem C.* 2013;117(51):27073–27080. doi:10.1021/jp409067h
46. Baffou G, Rigneault H. Femtosecond-pulsed optical heating of gold nanoparticles. *Phys Rev B.* 2011;84(3):035415. doi:10.1103/PhysRevB.84.035415
47. Hu M, Hartland GV. Heat dissipation for Au particles in aqueous solution: relaxation time versus size. *J Phys Chem B.* 2002;106(28):7029–7033.
48. Alper J, Hamad-schifferli K. Effect of ligands on thermal dissipation from gold nanorods. *Langmuir.* 2010;26(6):3786–3789. doi:10.1021/la904855s
49. Tolcher AW, Rodriguez VV, Rasco DW, et al. A Phase I study of the BCL2-targeted deoxyribonucleic acid inhibitor (DNAi) PNT2258 in patients with advanced solid tumors. *Cancer Chemother Pharmacol.* 2014;73(2):363–371. doi:10.1007/s00280-013-2361-0
50. Bastús NG, Comenge J, Puntès V. Kinetically controlled seeded growth synthesis of citrate-stabilized gold nanoparticles of up to 200 nm: size focusing versus Ostwald ripening. *Langmuir.* 2011;27(17):11098–11105. doi:10.1021/la201938u
51. Liu J, Lu Y. Preparation of aptamer-linked gold nanoparticle purple aggregates for colorimetric sensing of analytes. *Nat Protoc.* 2006;1(1):246. doi:10.1038/nprot.2006.38
52. Cho EC, Xie J, Wurm PA, Xia Y. Understanding the role of surface charges in cellular adsorption versus internalization by selectively removing gold nanoparticles on the cell surface with a 12/KI etchant. *Nano Lett.* 2009;9(3):1080–1084. doi:10.1021/nl803487r
53. Karimi S, Moshaii A, Abbasian S, Nikkha M. Surface plasmon resonance in small gold nanoparticles: introducing a size-dependent plasma frequency for nanoparticles in quantum regime. *Plasmonics.* 2018;14(4):851–860.
54. Saw WS, Ujihara M, Chong WY, et al. Size-dependent effect of cystine/citric acid-capped confetto-like gold nanoparticles on cellular uptake and photothermal cancer therapy. *Colloids Surf B.* 2018;161:365–374. doi:10.1016/j.colsurfb.2017.10.064
55. Wang S-H, Lee C-W, Chiou A, Wei P-K. Size-dependent endocytosis of gold nanoparticles studied by three-dimensional mapping of plasmonic scattering images. *J Nanobiotechnol.* 2010;8(1):33. doi:10.1186/1477-3155-8-33
56. Akrami M, Balalaie S, Hosseinkhani S, et al. Tuning the anticancer activity of a novel pro-apoptotic peptide using gold nanoparticle platforms. *Sci Rep.* 2016;6:31030. doi:10.1038/srep31030
57. Li H, Nelson E, Pentland A, Van Buskirk J, Rothberg L. Assays based on differential adsorption of single-stranded and double-stranded DNA on unfunctionalized gold nanoparticles in a colloidal suspension. *Plasmonics.* 2007;2(4):165–171. doi:10.1007/s11468-007-9032-0
58. Hunter RJ. *Foundations of Colloid Science.* Oxford university press; 2001.
59. Karni M, Zidon D, Polak P, Zalevsky Z, Shefi O. Thermal degradation of DNA. *DNA Cell Biol.* 2013;32(6):298–301. doi:10.1089/dna.2013.2056
60. Harrison E, Nicol JR, Macias-montero M, et al. A comparison of gold nanoparticle surface co-functionalization approaches using polyethylene glycol (PEG) and the effect on stability, non-specific protein adsorption and internalization. *Mater Sci Eng C.* 2016;62:710–718. doi:10.1016/j.msec.2016.02.003
61. Singh P, Pandit S, Mokkaapati V, Garg A, Ravikumar V, Mijakovic I. Gold nanoparticles in diagnostics and therapeutics for human cancer. *Int J Mol Sci.* 2018;19(7):1979. doi:10.3390/ijms19071979
62. Gilleron J, Querbes W, Zeigerer A, et al. Image-based analysis of lipid nanoparticle-mediated siRNA delivery, intracellular trafficking and endosomal escape. *Nat Biotechnol.* 2013;31(7):638. doi:10.1038/nbt.2612
63. Cobley CM, Chen J, Cho EC, Wang LV, Xia Y. Gold nanostructures: a class of multifunctional materials for biomedical applications. *Chem Soc Rev.* 2011;40(1):44–56. doi:10.1039/B821763G
64. Rosi NL, Giljohann DA, Thaxton CS, Lytton-jean AK, Han MS, Mirkin CA. Oligonucleotide-modified gold nanoparticles for intracellular gene regulation. *Science.* 2006;312(5776):1027–1030. doi:10.1126/science.1125559
65. Giljohann DA, Seferos DS, Patel PC, Millstone JE, Rosi NL, Mirkin CA. Oligonucleotide loading determines cellular uptake of DNA-modified gold nanoparticles. *Nano Lett.* 2007;7(12):3818–3821. doi:10.1021/nl072471q
66. Patel PC, Giljohann DA, Daniel WL, Zheng D, Prigodich AE, Mirkin CA. Scavenger receptors mediate cellular uptake of polyvalent oligonucleotide-functionalized gold nanoparticles. *Bioconjug Chem.* 2010;21(12):2250–2256. doi:10.1021/bc1002423
67. Seferos DS, Prigodich AE, Giljohann DA, Patel PC, Mirkin CA. Polyvalent DNA nanoparticle conjugates stabilize nucleic acids. *Nano Lett.* 2009;9(1):308–311. doi:10.1021/nl802958f
68. Giljohann DA, Seferos DS, Prigodich AE, Patel PC, Mirkin CA. Gene regulation with polyvalent siRNA-nanoparticle conjugates. *J Am Chem Soc.* 2009;131(6):2072–2073. doi:10.1021/ja808719p
69. Ebrahim AS, Kandouz M, Emara N, Sugalski AB, Lipovich L, Alkatib AM. Unintended target effect of anti-BCL-2 DNAi. *Cancer Manag Res.* 2017;9:427. doi:10.2147/CMAR.S139105
70. Anderson RR, Parrish JA. Selective photothermolysis: precise microsurgery by selective absorption of pulsed radiation. *Science.* 1983;220(4596):524–527. doi:10.1126/science.6836297
71. Jain PK, Lee KS, El-Sayed IH, El-sayed MA. Calculated absorption and scattering properties of gold nanoparticles of different size, shape, and composition: applications in biological imaging and biomedicine. *J Phys Chem B.* 2006;110(14):7238–7248. doi:10.1021/jp057170o
72. Johnson PB, Christy R-W. Optical constants of the noble metals. *Phys Rev B.* 1972;6(12):4370. doi:10.1103/PhysRevB.6.4370

International Journal of Nanomedicine

Dovepress

Publish your work in this journal

The International Journal of Nanomedicine is an international, peer-reviewed journal focusing on the application of nanotechnology in diagnostics, therapeutics, and drug delivery systems throughout the biomedical field. This journal is indexed on PubMed Central, MedLine, CAS, SciSearch[®], Current Contents[®]/Clinical Medicine,

Journal Citation Reports/Science Edition, EMBase, Scopus and the Elsevier Bibliographic databases. The manuscript management system is completely online and includes a very quick and fair peer-review system, which is all easy to use. Visit <http://www.dovepress.com/testimonials.php> to read real quotes from published authors.

Submit your manuscript here: <https://www.dovepress.com/international-journal-of-nanomedicine-journal>